Title
Distinct Populations of Innate CD8+ T Cells Revealed in a CXCR3 Reporter Mouse

Journal
The Journal of Immunology, 190(5)

ISSN
0022-1767

Authors
Oghumu, Steve
Dong, Ran
Varikuti, Sanjay
et al.

Publication Date
2013-03-01

DOI
10.4049/jimmunol.1201170

Peer reviewed

Published in final edited form as:
J Immunol. 2013 March 1; 190(5): 2229–2240. doi:10.4049/jimmunol.1201170.

Distinct Populations of Innate CD8+ T Cells Revealed in a CXCR3 Reporter Mouse

Steve Oghumu[*,†], **Ran Dong**[*], **Sanjay Varikuti**[*], **Todd Shawler**[‡], **Thomas Kampfrath**[§], **Cesar A. Terrazas**[*], **Claudio Lezama-Davila**[*], **Brian M. M. Ahmer**[¶], **Caroline C. Whitacre**[‡], **Sanjay Rajagopalan**[§], **Richard Locksley**[‖], **Arlene H. Sharpe**[#], and **Abhay R. Satoskar**[*]

[*]Department of Pathology, The Ohio State University Medical Center, Columbus, OH 43210

[†]Department of Oral Biology, The Ohio State University College of Dentistry, Columbus, OH 43210

[‡]Department of Molecular Virology, Immunology, and Medical Genetics, The Ohio State University, Columbus, OH 43210

[§]Department of Microbiology and Immunology, Davis Heart and Lung Research Institute, The Ohio State University College of Medicine, Columbus, OH 43210

[¶]Department of Microbiology, The Ohio State University, Columbus, OH 43210

[‖]Howard Hughes Medical Institute, University of California San Francisco, San Francisco, CA 94143

[#]Department of Pathology, Harvard Medical School, Brigham and Women's Hospital, Boston, MA 02115

Abstract

CXCR3, expressed mainly on activated T and NK cells, is implicated in a host of immunological conditions and can contribute either to disease resolution or pathology. We report the generation and characterization of a novel CXCR3 internal ribosome entry site bicistronic enhanced GFP reporter (CIBER) mouse in which enhanced GFP expression correlates with surface levels of CXCR3. Using CIBER mice, we identified two distinct populations of innate $CD8^+$ T cells based on constitutive expression of CXCR3. We demonstrate that $CXCR3^+$ innate $CD8^+$ T cells preferentially express higher levels of Ly6C and CD122, but lower levels of CCR9 compared with $CXCR3^-$ innate $CD8^+$ T cells. Furthermore, we show that $CXCR3^+$ innate $CD8^+$ T cells express higher transcript levels of antiapoptotic but lower levels of proapoptotic factors, respond more robustly to IL-2 and IL-15, and produce significantly more IFN-γ and granzyme B. Interestingly, $CXCR3^+$ innate $CD8^+$ T cells do not respond to IL-12 or IL-18 alone, but produce significant amounts of IFN-γ on stimulation with a combination of these cytokines. Taken together, these findings demonstrate that $CXCR3^+$ and $CXCR3^-$ innate $CD8^+$ T cells are phenotypically and functionally distinct. These newly generated CIBER mice provide a novel tool for studying the role of CXCR3 and CXCR3-expressing cells in vivo.

Address correspondence and reprint requests to Dr. Abhay R. Satoskar, Department of Pathology, The Ohio State University Medical Center, 129 Hamilton Hall, 1645 Neil Avenue, Columbus, OH 43210. abhay.satoskar@osumc.edu.

The online version of this article contains supplemental material.

Disclosures

The authors have no financial conflicts of interest.

The chemokine receptor CXCR3 is preferentially expressed on activated Th1 cells, $CD8^+$ T cells, NK cells, NKT cells, natural regulatory T cells, as well as microvascular endothelial cells in the S/G_2-M phase of their life cycle (1). In lymphocytic cells, expression of CXCR3 is generally inducible, although constitutive CXCR3 expression in NK and NKT cells of naive, uninfected mice have been observed (1). Three CXC chemokines, CXCL9 (MIG), CXCL10 (IP-10), and CXCL11 (I-TAC), signal via CXCR3 (1) and mediate biological functions such as cell migration and proliferation.

It is well documented that CXCR3 and its ligands play a critical role in immunity and resolution of infections caused by a variety of pathogens. For example, CXCR3 expression on activated T lymphocytes is essential to the resolution of a number of parasitic, bacterial, viral, and fungal infections including *Leishmania major* and HSV type 1 infections (2, 3). In most instances, CXCR3 mediates recruitment of T cells involved in Th1 type immunity to peripheral sites of infection. However, in some infectious and autoimmune diseases, CXCR3-expressing immune cells contribute to immunopathology (4, 5). Recent studies have also implicated protective as well as detrimental roles for CXCR3 in cancer (6). These studies point to diverse functions for CXCR3-expressing cell populations in animal models of autoimmune, neoplastic, and infectious diseases. However, investigation of the role of CXCR3 in infection in vivo or functional analysis of CXCR3-expressing cells ex vivo has been difficult because of the lack of appropriate tools for tracking and/or isolating CXCR3-expressing cells.

To study the role of CXCR3-expressing cells in vivo, we have generated and characterized a CXCR3 internal ribosome entry site bicistronic enhanced GFP reporter (CIBER) mouse using a bicistronic reporter system as described previously (7). CIBER mice are truly CXCR3 reporter mice, as all CXCR3-expressing cells in these mice also express enhanced GFP (EGFP). Using these mice, we have identified phenotypically and functionally distinct populations of innate $CD8^+$ T cells based on CXCR3 expression. Innate $CD8^+$ T cells, which are found in naive mice, develop via a different pathway from conventional $CD8^+$ T cells (8–10). They phenotypically resemble bona fide memory $CD8^+$ T cells and require IL-15 for their homeostatic maintenance (11). Several studies have shown that innate $CD8^+$ T cells contribute to early host defenses against a variety of pathogens including *Listeria monocytogenes*, *Salmonella typhimurium*, and *Mycobacterium tuberculosis* (12). To our knowledge, our study is the first to reveal two distinct subsets of these nonconventional $CD8^+$ T cells. CIBER mice should provide a valuable tool for researchers to study the role of CXCR3, as well as its regulation in vivo.

Materials and Methods

Mouse strains and infection protocol

All wild-type (WT) and knockout C57BL/6 mice were purchased from The Jackson Laboratory (Bar Harbor, ME) and maintained in a pathogen-free animal facility at The Ohio State University in accordance with National Institutes of Health and institutional guidelines. Mice were infected either with 2×10^8 *S. typhimurium* (*aroA*$^{-/-}$ strain) orally, 2×10^5 *Histoplasma* yeast strain G217B intranasally, or 2×10^6 *L. major* promastigotes s.c. in their hind footpad. Mice were sacrificed at the indicated times postinfection, and single-cell suspensions from Peyer's patches, spleens, and lungs were prepared and analyzed by flow cytometry for the presence of GFP^+ cells.

Intravital microscopy

Male CIBER mice were sensitized using the contact hypersensitivity (CHS) model with dinitrofluorobenzene (DNFB) as described previously (13), then challenged 6 d later on the

skin surface over the cremaster muscle or on the ear dermis. Sixteen hours later, mice were anesthetized using tribromoethanol. Under anesthesia, the testicular cremaster muscle was surgically exposed using a dissecting microscope (2×; Nikon SMZ 645; Nikon, Tokyo, Japan) and mounted on a coherent cube. The cremaster muscle was bathed with Ringer's lactate at 37°C, and leukocyte endothelial interaction was assessed in 5–10 venules using a Nikon Eclipse FN1 microscope (Nikon) with a 40×/0.80 W water immersed objective at a 2.0-mm working distance. Video images were captured and digitalized to 12-bit TIF images using MetaMorph software (version 7.1.2.0; MetaMorph, Downingtown, PA).

For CIBER mouse ear imaging, mouse was anesthetized and the inflamed ear dermis was visualized using a Zeiss LSM 700 confocal laser-scanning microscope. Fluorescent images were acquired as Z-stacks and three-dimensional images were generated using Zen software (Carl Zeiss MicroImaging, Jena, Germany).

In vitro T cell activation

Cells for in vitro T cell activation were obtained from excised lymph nodes and spleens of uninfected mice or from sorted populations using BD FACSAria cell sorter (Becton-Dickinson Biosciences, San Jose, CA). Splenocytes were incubated with Boyle's solution at room temperature for 10 min to lyse RBCs, then washed with RPMI 1640 supplemented with 10% FBS. Enriched T cell populations were obtained by passing cell suspensions through nylon wool columns. Purified T cells or $CD8^+$ $CD44^+$ $CD62L^+$ sorted cells were incubated at $0.5–2.5 \times 10^6$ cells/well with plate-bound anti-CD3 (3 μg/ml, clone 145–2C11) and anti-CD28 (4 μg/ml, clone 37.51) Abs (BioLegend, San Diego, CA) or with recombinant mouse cytokines (R&D Systems, Minneapolis, MN) for 48 h. After in vitro activation, cells were either rested in their conditioned media and analyzed by flow cytometry using PE-labeled anti-mouse CXCR3 Ab (BioLegend, San Diego, CA) or collected for real-time PCR analysis and ELISA of culture supernatants.

In vivo proliferation assays

Sorted $CXCR3^+$ and $CXCR3^-$ innate $CD8^+$ T cells from WT, CIBER, or OT1-CIBER mice were stained with CellTrace Violet (Invitrogen, Carlsbad CA) according to the manufacturer's instructions. Labeled cells were then injected i.v. into Thy1.1 recipient mice via the tail vein. The next day, recipient mice were injected with OVA, OVA/CFA, PBS/CFA, or PBS at the hind footpad. On day 3 postimmunization, draining popliteal lymph nodes were harvested and analyzed for proliferation by flow cytometry.

Migration assays

T cells from the spleens and lymph nodes of naive WT, CIBER, and *cxcr3*$^{-/-}$ mice were isolated and activated in vitro with plate-bound anti-CD3 and -CD28 Abs for 48 h. Cells were then subsequently recultured in fresh media (in the absence of CD3/CD28 stimulation) for 48 h to induce CXCR3 expression in WT and CIBER mice T cells (14). For in vivo migration assays, $CXCR3^+$ T cells from WT and CIBER mice, as well as T cells from *cxcr3*$^{-/-}$ mice, were labeled with cell tracking dyes Qdot 655, Qdot 800, and Qdot 585, respectively, using the Qtracker Cell Labeling Kit (Invitrogen, Carlsbad, CA). Equal numbers were adoptively transferred to WT recipient mice. Twenty-four hours later, 10 μg CXCL10 in 50 μl was injected intratracheally into recipient mice. After another 24 h, mice were sacrificed and infiltrating cells in the lungs were isolated by bronchoalveolar lavage, then analyzed using BD FACS Canto flow cytometer (Becton-Dickinson Biosciences). Migration in DNFB-sensitized WT and CIBER mice was performed as described earlier for CIBER mouse ear imaging. Cells from mouse ears were obtained as described previously (15). In brief, mouse ear dorsal and ventral dermal sheets were separated and incubated dermal side down in culture media containing 2 mg/ml collagenase A and 0.5 mg/ml DNase

I for 2 h at 37°C, then passed through a 70-μm strainer to obtain single-cell suspensions. Cells were stained with CD3 and CD8 Abs and analyzed by flow cytometry using a FACSCalibur flow cytometer (Becton-Dickinson Biosciences).

In vitro migration assays were performed as described previously (16). In brief, dilutions of chemokine in media were added to the bottom of 96-well chemotaxis plates (Corning). A total of 5×10^4 $CXCR3^+$ T cells was added to the top of the membrane and incubated at 37°C for 2 h. Cells in the bottom wells were subsequently counted using a microscope. Results were presented as chemotactic indices by dividing the number of cells in the bottom well in response to the chemokine by the average number of cells in the bottom well without the addition of chemokines.

Statistical analysis

Student unpaired *t* test was used to determine statistical significance of values obtained. The *p* values <0.01 were considered statistically significant.

Results

Generation of CIBER mice and validation of GFP production by CXCR3-expressing cells

To examine the role of CXCR3-expressing cells during infection and inflammation in vivo, we generated and characterized a CXCR3 knock-in reporter (CIBER) mouse. A CXCR3 bicistronic reporter targeting vector was designed for integration by homologous recombination into the CXCR3 locus. A 13-kb mouse genomic fragment of the CXCR3 locus consisting of exons 1 and 2, a 5.8-kb flanking sequence and a 3.4-kb flanking sequence at the 5′ and 3′ ends of the coding region, respectively, was used to generate the targeting vector. The vector was modified by introducing an internal ribosome entry site element, EGFP, and a bovine growth hormone polyadenylation signal, followed by a loxP flanked neomycin cassette downstream of the translational stop codon and upstream of the endogenous polyadenylation signal in the 3′ untranslated region of exon 2. A herpes simplex thymidine kinase cassette was cloned to one flank of the targeting construct to serve as a counter-selectable marker for targeted integration. The linearized targeting vector was electroporated into 129SvE embryonic stem cells. G418-resistant and ganciclovir-sensitive clones were screened by Southern blot for targeted integration into the CXCR3 locus (Fig. 1A, 1B). Mouse PCR genotyping revealed a 222-bp band for CIBER mice or a 448-bp band for WT mice, whereas heterozygous mice showed both bands (Fig. 1C). All mice were viable and healthy with no phenotypic defects. We have designated these mice as CIBER mice.

T cells that have been shown to express CXCR3 on activation by plate-bound anti-CD3 and anti-CD28 Abs, and subsequent re-culture in conditioned medium in the absence of external stimuli (14). To determine whether surface expression of CXCR3 on the cells from CIBER mice correlated with EGFP production, we activated T cells of WT, *cxcr3*$^{-/-}$, or CIBER mice using anti-CD3/anti-CD28 as described previously (17), and analyzed expression of EGFP in $CXCR3^+$ T cells stained using PE-conjugated anti-CXCR3 Ab. We found that in vitro–activated splenic T cells from CIBER mice that expressed CXCR3 on their surface also expressed EGFP (Fig. 1D). Levels of CXCR3 protein expression in CIBER mice were comparable with that of WT mice after in vitro T cell activation (Fig. 1D). Moreover, expression of CXCR3 in T cells was proportionate to EGFP production, and EGFP fluorescence was undetectable in the cells that did not express surface CXCR3. A similar expression pattern was observed in lymph node cells of CIBER mice. Taken together, these data show that CIBER mouse is a reliable reporter for CXCR3 expression.

Migration of CXCR3-expressing cells to inflamed tissues in vivo is not compromised in CIBER mice

Next, we examined whether CXCR3-expressing cells could be visualized in vivo during inflammation in real time in live mice. To do this, we elicited DNFB-mediated CHS in the skin over the groin of male CIBER mice and analyzed recruitment of GFP-expressing cells in the underlying cremasteric tissue by intravital microscopy (Fig. 2A). CXCR3-expressing ($EGFP^+$) cells recruited into the inflamed tissue and tethered to the endothelial vessel wall of inflamed postcapillary venules in surgically exposed testicular cremaster muscle were readily visible (Fig. 2A). Similar results were obtained when CHS was induced in the ear dermis of CIBER mice (Fig. 2B). To further validate the use of CIBER mice in studying recruitment of $CXCR3^+$ cells to different anatomical sites, we analyzed $EGFP^+$ cells at infection sites of CIBER mice challenged intranasally with *Histoplasma capsulatum* or orally with *S. typhimurium*. $EGFP^+$ cells were readily detectable in inflamed lung tissues of *Histoplasma*-infected, as well as in Peyer's patches of *S. typhimurium*-infected, CIBER mice by flow cytometry (Fig. 2C). These findings demonstrate that $CXCR3^+$ cells in CIBER mice have the ability to migrate to inflamed tissues, and that these cells can be tracked in vivo during inflammation and infection.

Further, we determined whether there was any defect in the migration of $CXCR3^+$ cells in CIBER mice as a result of insertion of the EGFP reporter gene into the CXCR3 locus. We therefore compared the migration of $CXCR3^+$ cells in WT and CIBER mice using in vivo and in vitro models. $CD8^+$ T cell recruitment to the ear dermis after DNFB mediated CHS induction of WT and CIBER mice was observed to be identical in both mice (Fig. 3A, 3B). In another in vivo model, $CXCR3^+$ T cells from WT and CIBER mice, as well as T cells from *cxcr3*$^{-/-}$ mice, were labeled with different cellular tracking dyes and adoptively transferred to WT recipient mice. Recruitment to the lungs was analyzed after intratracheal administration of the CXCR3 ligand CXCL10. Flow cytometric analysis of lung infiltrates revealed similar numbers of adoptively transferred T cells from WT and CIBER mice, but not *cxcr3*$^{-/-}$ mice (Fig. 3C, 3D). To further demonstrate that migration of CXCR3-expressing cells in CIBER mice is not compromised, we compared migration of $CXCR3^+$ T cells from WT and CIBER mice, as well as T cells from *cxcr3*$^{-/-}$ mice, with the CXCR3 ligands CXCL9, CXCL10, and CXCL11 in vitro. As with in vivo migration models, migration of $CXCR3^+$ T cells to all CXCR3 ligands was similar in WT and CIBER mice (Fig. 3E–G). Furthermore, sorted T cells from WT and CIBER mice produced similar proliferative responses and cytokine levels after TCR or antigenic stimulation (Supplemental Fig. 1). Taken together, these findings demonstrate that $CXCR3^+$ cells in CIBER mice have no functional or chemotactic defects.

Detection of CXCR3-expressing cells in naive CIBER mice

Previous reports have shown that CXCR3 is expressed on NK cells, NKT cells, and T cells in mice (18). Analysis of secondary lymphoid organs from naive CIBER mice, as well as anti-CXCR3 Ab staining of naive WT mice, confirmed expression of CXCR3 by these cell populations (Fig. 4A–C). In addition, we found expression of CXCR3 in a small population of B lymphocytes (Fig. 4D). CXCR3 expression on Ab-secreting cells of virally infected mice has been previously reported (19), but the significance of CXCR3 expression on B lymphocytes in naive, uninfected mice is yet to be fully understood, although these cells are likely to be memory B cells. Furthermore, in CIBER mice infected with *L. major*, we observed a general increase in the expression of CXCR3 in lymphocytes (Supplemental Fig. 2).

CXCR3 is generally an inducible receptor, although constitutive expression in innate lymphocytes including NK and NKT cells is well documented (18). Our analysis of CIBER

mice revealed that, in addition to these subsets, a majority of CXCR3-expressing lymphocytes in the lymphoid organs of naive mice expressed the CD8 coreceptor (Fig. 4B). These CXCR3-expressing $CD8^+$ T cells also expressed CD62L and CD44, suggesting similar characteristics with some central memory T cells (Fig. 4E). However, these populations were detected in uninfected naive mice, as well as in naive germ-free mice (Fig. 5A, 5B), and therefore could not be bona fide memory $CD8^+$ T cells. Naturally occurring "memory phenotype" $CD8^+$ T cells that originate from similar $CD4^+CD8^+$ thymocyte progenitors as with conventional naive $CD8^+$ T cells but with a different lineage have been reported (8, 11). The phenotypic characteristics displayed by the CXCR3-expressing "memory phenotype" $CD8^+$ T lymphocytes in naive CIBER mice are similar to these nonconventional innate $CD8^+$ T cells. Of note, only about half of the innate $CD8^+$ T cells in naive mice expressed CXCR3, suggestive of potential phenotypic differences between the $CXCR3^+$ and $CXCR3^-$ populations of innate $CD8^+$ T cells (Fig. 5A).

Role of STAT1, IFN-γ, and T-bet in CXCR3 expression by innate $CD8^+$ T cells

Given the constitutive nature of CXCR3 expression in a population of innate $CD8^+$ T cells observed in naive CIBER mice, we determined whether T-bet, STAT-1, or IFN-γ were essential for the expression of CXCR3 on these cells. It is well established that expression of CXCR3 on activated T cells is tightly regulated by the transcription factor and master regulator of Th1 differentiation and function, T-bet (20). We have also previously shown that IFN-γ and STAT-1 are critical for the efficient induction of CXCR3 in $CD4^+$, but not $CD8^+$, T cells on activation (17). To determine whether STAT1 and/or T-bet are required for CXCR3 expression on innate $CD8^+$ T cells, we analyzed innate $CD8^+$ T cells isolated from the spleens and lymph nodes of naive *T-bet*$^{-/-}$, *stat1*$^{-/-}$, and *ifn-γ*$^{-/-}$ mice for cellular CXCR3 expression by flow cytometry. $CXCR3^+$ innate $CD8^+$ T cells were present in all groups of mice (Fig. 5C, 5D). However, the proportion of $CXCR3^+$ innate $CD8^+$ T cells was slightly reduced in *T-bet*$^{-/-}$ mice compared with WT mice (Fig. 5C, 5D). Taken together, our results show that T-bet might contribute to the expression of CXCR3 in innate $CD8^+$ T cells. However, T-bet does not seem to be required for the presence of this population.

$CXCR3^+$ and $CXCR3^-$ innate $CD8^+$ T populations possess distinct phenotypic characteristics

Although antigenic diversity within the innate $CD8^+$ T cell repertoire has been described, phenotypic and functional classifications of this population are poorly characterized. As noted earlier, we observed that not all innate $CD8^+$ T cells in naive mice express CXCR3. This led us to examine whether phenotypic differences exist between $CXCR3^+$ and $CXCR3^-$ populations of innate $CD8^+$ T cells. We therefore isolated $CXCR3^+$ and $CXCR3^-$ innate CD8s, as well as naive $CD8^+$ T cells, from uninfected CIBER mice, then analyzed their gene expression profiles. We observed that $CXCR3^+$ innate $CD8^+$ T cells display higher levels of *T-bet* and *IFN-γ* mRNA compared with $CXCR3^-$ innate CD8, suggesting a greater potential for this population to produce IFN-γ (Fig. 6A). Differences in the expression of genes involved in T cell development and function were also observed between both populations of innate $CD8^+$ T cells, including higher levels of Spi-6, Spi-2a, GATA-3, and IL-10, and lower levels of Id-2, Notch, PD-1, and CTLA-4 expressed by $CXCR3^+$ innate CD8 T cells (Fig. 6A).

To further characterize phenotypic differences between $CXCR3^+$ and $CXCR3^-$ innate $CD8^+$ T cells, we analyzed the expression of cell-surface markers by both populations. $CXCR3^+$ innate $CD8^+$ T cells expressed significantly greater levels of Ly6C than $CXCR3^-$ innate $CD8^+$ T cells (Fig. 6B). We also observed significant differences in the cell-surface expression of IL-2Rβ, a receptor for IL-2 and IL-15, which was consistently higher in $CXCR3^+$ innate $CD8^+$ T cells (Fig. 6B). This finding suggests that subsets of innate $CD8^+$ T

cells have varied responses to IL-2 and IL-15. Taken together, our results demonstrate that CXCR3$^+$ and CXCR3$^-$ innate CD8 T cells possess distinct phenotypic characteristics.

CXCR3$^+$ innate CD8$^+$ T cells proliferate more robustly and produce greater levels of IFN-γ and granzyme B on stimulation

Innate CD8$^+$ T cells generally display a more activated surface phenotype and respond more rapidly to TCR stimulation than conventional naive CD8$^+$ T cells (8). Furthermore, they have the ability to produce IFN-γ in response to cytokine stimulation without TCR engagement (10). As such, they play a significant role in early innate responses against bacterial infection before the onset of adaptive immunity (12). Because we observed phenotypic and transcriptional differences between CXCR3$^+$ and CXCR3$^-$ innate CD8$^+$ T cells, we determined whether functional differences exist in both populations. Given that CXCR3 expression is associated with activated T cells, we hypothesized that CXCR3$^+$ innate CD8$^+$ T cells would display a more activated and proliferative phenotype than those not expressing CXCR3. To test this hypothesis, single-cell suspensions from spleen and lymph nodes of naive CIBER mice were stimulated with IL-12/IL-18, IL-12/IL-15, IL-12/IL-2, or PMA/ionomycin, then analyzed for surface expression of activation markers and intracellular IFN-γ production. In addition, naive, CXCR3$^+$, and CXCR3$^-$ innate CD8$^+$ T cells were sorted and stimulated with anti-CD3/CD28 Abs, IL-12/IL-18, IL-12/IL-15, and IL-12/IL-2, then analyzed for proliferation, gene expression, and IFN-γ production. On stimulation with anti-CD3/CD28, CXCR3$^+$ innate CD8$^+$ T cells produced significantly greater amounts of IFN-γ than in CXCR3$^-$ innate CD8$^+$ T cells or naive CD8$^+$ T cells (Fig. 7A). Similar results were observed using intracellular staining of IFN-γ after PMA/ionomycin stimulation (Fig. 7B). Cellular stimulation with IL-12/IL-2, IL-12/IL-15, and IL-12/IL-18 cytokine combinations also resulted in greater IFN-γ production (Fig. 7C, 7D) and increased cell-surface expression of activation markers CD25 and CD69 (Fig. 8A, 8B) by CXCR3$^+$ innate CD8$^+$ T cells. Furthermore, real-time PCR analysis revealed that increased IFN-γ production by CXCR3$^+$ innate CD8$^+$ T cells correlates with a significant induction of IFN-γ mRNA in these cells (Fig. 8C). Stimulation with IL-12/IL-15 and IL-12/IL-2 also resulted in significantly greater granzyme B induction (Fig. 8C), as well as proliferation of CXCR3$^+$ innate CD8$^+$ T cells (Fig. 8D). Interestingly, combination of IL-12/IL-18 also increased IFN-γ production by CXCR3$^+$ innate CD8$^+$ T cells (Fig. 7C, 8C), but unlike IL-12/IL-15 and IL-12/IL-2, it did not induce the proliferation of these cells (Fig. 8D).

To confirm this functional difference in the proliferative response of these cells to antigenic stimulation in vivo, we sorted CXCR3$^+$ and CXCR3$^-$ innate CD8$^+$ T cells from OT1-CIBER mice, labeled them with CellTrace Violet Cell Proliferation kit, and then adoptively transferred them to WT Thy1.1 recipients. Proliferative responses of transferred cells in the draining lymph node were analyzed after injection of recipient mice with OVA. Consistent with our in vitro results, CXCR3$^+$ innate CD8$^+$ T cells proliferated more robustly than CXCR3$^-$ innate CD8$^+$ T cells (Fig. 8E). Proliferative responses and cytokine production of sorted CXCR3$^+$ or CXCR3$^-$ innate CD8$^+$ T cell populations to in vitro stimulation from WT mice were similar to those observed in CIBER mice (Supplemental Fig. 3). Taken together, our results suggest that CXCR3$^+$, but not CXCR3$^-$, innate CD8$^+$ T cells could be involved in the generation of a more rapid effector response after antigenic or cytokine stimulation.

IL-2 and IL-15 enhance the effector functions of CXCR3-expressing innate CD8$^+$ T cells

Our observation that surface expression of IL-2Rβ (a coreceptor for IL-2 and IL-15) is greater among CXCR3$^+$ innate CD8$^+$ T cells led us to examine whether both populations differ in their response to in vitro stimulation by IL-2 or IL-15 alone. Numerous studies have demonstrated a requirement for IL-15 in the homeostatic maintenance and functions of

innate $CD8^+$ T cells (8–11), and these cells have been shown to proliferate in vitro to IL-2 alone (21, 22). However, the ability of IL-2 or IL-15 alone to induce the production of effector molecules by innate $CD8^+$ T cells independent of Ag has not been fully explored. In view of the observed variation in response to mixed cytokine stimulation, we stimulated splenocytes and lymph node cells with IL-2, IL-12, IL-15, or IL-18 alone, and analyzed intracellular IFN-γ production by flow cytometry. We observed that $CXCR3^+$ innate $CD8^+$ T cells preferentially responded to IL-2 or IL-15 stimulation by producing greater amounts of intracellular IFN-γ than $CXCR3^-$ innate $CD8^+$ T cells (Fig. 9A).

Because whole-spleen and lymph-node cell preparations also contain other immune cells that could influence responsiveness of innate $CD8^+$ T cells to cytokines and affect CXCR3 expression, we isolated $CXCR3^+$ and $CXCR3^-$ innate $CD8^+$ T cells from naive CIBER mice by FACS sorting and subjected them to similar cytokine stimulation conditions. Consistent with our previous data, we observed a much higher induction of IFN-γ and granzyme B mRNAs in $CXCR3^+$ innate $CD8^+$ T cells after stimulation with IL-2 and IL-15, but not IL-12 and IL-18 (Fig. 9C). Furthermore, $CXCR3^+$ innate $CD8^+$ T cells secreted greater amounts of IFN-γ (Fig. 9B), and showed greater proliferation (Fig. 9D), than cells not expressing CXCR3 after stimulation with IL-2 or IL-15, but not IL-12 or IL-18. However, we did not observe any significant differences in the expression of c-myc, and bcl-2 transcripts were lower in $CXCR3^+$ innate $CD8^+$ T cells than in $CXCR3^-$ innate $CD8^+$ and naive $CD8^+$ T cells after IL-2 and IL-15 stimulation (data not shown). Taken together, these findings confirm the functional differences that exist between $CXCR3^+$ and $CXCR3^-$ innate $CD8^+$ T cells.

Discussion

Bicistronic reporter mouse models that characterize immune-related gene-expressing cells are valuable tools that greatly enhance our understanding of gene regulation, function, and cellular expression in vivo. This system has been successfully used to examine the roles of IL-4, IL-10, and FoxP3, and their contribution to the immune response (7, 23, 24). Our data demonstrate that CIBER mouse is an ideal reporter system for CXCR3 expression, because EGFP production correlates with CXCR3 expression levels. Unlike cytokines that could potentially be stored within the cell before release, CXCR3 is primarily regulated at the transcriptional level (25). Furthermore, unlike other chemokine receptors, CXCR3 is not recycled back to the cell surface after constitutive or ligand-induced internalization but is rapidly degraded. As such, replenishment of cell-surface CXCR3 is dependent on de novo synthesis of CXCR3 protein and subsequent transport through the Golgi (25). This makes CXCR3 mRNA transcript levels a suitable indicator for cell-surface expression of the CXCR3 protein, which is the basis for the EGFP bicistronic reporter system in CIBER mice. Our model also facilitates sorting of CXCR3-expressing cells without interfering with cell-surface CXCR3 expression and function, which could be induced by binding with anti-CXCR3 Abs.

In this study, using CIBER mice, we identified $CXCR3^+$ and $CXCR3^-$ populations of innate $CD8^+$ T cells that are transcriptionally and phenotypically distinct. $CXCR3^+$ innate $CD8^+$ T cells expressed higher transcript levels of Spi-6 and Spi-2a and lower levels of PD-1 than $CXCR3^-$ innate $CD8^+$ T cells. The serine protease inhibitors Spi-6 and Spi-2a have been shown to block the activity of granzyme B and cathepsin B and favor the longevity of memory T cells (26, 27). Downregulation of the inhibitory receptor, PD-1, is crucial to the formation of functional memory $CD8^+$ T cells after acute infection (28). The pattern of gene expression displayed by $CXCR3^+$ innate $CD8^+$ T cells appears to be similar to those of bona fide central memory $CD8^+$ T cells, favoring long-term persistence and preventing apoptosis (29). Therefore, the roles played by $CXCR3^+$ innate $CD8^+$ T cells during the innate phase of

an immune response might very well be comparable with the functions of central memory $CD8^+$ T cells during adaptive immunity to recall infections.

We observed significant differences in the surface expression of Ly6C between $CXCR3^+$ and $CXCR3^-$ populations of innate $CD8^+$ T cells. Ly6C is involved in signal transduction and cytokine production during T cell activation and has recently been shown to play a role in the trafficking of central memory T cells (30). Its function in $CXCR3^+$ innate $CD8^+$ T cells is not clear, but it is possible that Ly6C plays similar functional and migratory roles. Indeed, migratory differences are further suggested by our observation that CCR9, a gut homing chemokine receptor, is down-regulated in the $CXCR3^+$ innate $CD8^+$ T cells compared with innate $CD8^+$ T cells that do not express CXCR3 (Fig. 6A).

$CXCR3^+$ innate $CD8^+$ T cells showed higher cell-surface expression of IL-2Rβ. IL-2 and IL-15 signal through IL-2Rβ (CD122), a common cytokine receptor γ subunit (CD132) and a cytokine-specific α-chain (31). Memory T cells express IL-2Rβ, and the expression of this receptor on innate $CD8^+$ T cells, as well as the dependence of this population on IL-15 for homeostatic maintenance, has been reported (11). However, we observe differential expression of IL-2Rβ among innate $CD8^+$ T cells correlating with the expression of CXCR3 on these cells. Our results suggest that $CXCR3^+$ innate $CD8^+$ T cells are more responsive than $CXCR3^-$ innate $CD8^+$ T cells to IL-2– and IL-15–mediated signaling, resulting in increased cell proliferation, activation, and induction of effector genes. Signal transduction through IL-2Rβ involves the Jak1, Jak3, STAT3, and STAT5 (31). PI3K/AKT and Ras/Raf/MAPK pathways are also stimulated, leading to the induction of *c-myc*, *bcl-2*, and *c-fos/c-jun*, which promotes cell survival, proliferation, and cytotoxic activity of $CD8^+$ memory T cells and NK cells (32, 33). However, because we did not observe increased levels of c-myc and bcl-2 transcripts in $CXCR3^+$ innate $CD8^+$ T cells, it is possible that other signaling pathways are induced in $CXCR3^+$ innate $CD8^+$ T cells after stimulation with these cytokines.

In conclusion, we demonstrate, using our newly generated CIBER mice, the existence of distinct populations of innate $CD8^+$ T cells that differ in activation status, transcriptional profile, and surface marker expression based on the expression of the chemokine receptor CXCR3, which suggests distinct functional and phenotypic characteristics. Targeting this population of innate $CD8^+$ T cells may provide an early source of IFN-γ during intracellular bacterial infections before the onset of adaptive immunity. We believe that CIBER mouse will further enable assessment of the contributions made by various CXCR3-expressing cell populations to the overall immune response in a variety of infectious, autoimmune, and neoplastic diseases.

Supplementary Material

Refer to Web version on PubMed Central for supplementary material.

Acknowledgments

This work was supported by National Institute of Dental and Craniofacial Research Training Grant T32DE014320 (to S.O.), National Institutes of Health Grants R03AI090231 (to A.R.S.) and R56AI068829 (to A.R.S.), and Grants R21DK088522 (to S.R.) and R01017290 (to S.R.).

We thank Dr. Jessica Edwards, Matthew Swearingen, Dr. Chad Rappleye, and Dmitri Kotov for technical contributions.

Abbreviations used in this article

CHS	contact hypersensitivity
CIBER	CXCR3 internal ribosome entry site bicistronic enhanced GFP reporter
DNFB	dinitrofluorobenzene
EGFP	enhanced GFP
WT	wild-type

References

1. Groom JR, Luster AD. CXCR3 ligands: redundant, collaborative and antagonistic functions. Immunol Cell Biol. 2011; 89:207–215. [PubMed: 21221121]
2. Carr DJ, Wuest T, Ash J. An increase in herpes simplex virus type 1 in the anterior segment of the eye is linked to a deficiency in NK cell infiltration in mice deficient in CXCR3. J Interferon Cytokine Res. 2008; 28:245–251. [PubMed: 18439102]
3. Rosas LE, Barbi J, Lu B, Fujiwara Y, Gerard C, Sanders VM, Satoskar AR. CXCR3$^{-/-}$ mice mount an efficient Th1 response but fail to control *Leishmania major* infection. Eur J Immunol. 2005; 35:515–523. [PubMed: 15668916]
4. Mohan K, Issekutz TB. Blockade of chemokine receptor CXCR3 inhibits T cell recruitment to inflamed joints and decreases the severity of adjuvant arthritis. J Immunol. 2007; 179:8463–8469. [PubMed: 18056393]
5. Campanella GS, Tager AM, El Khoury JK, Thomas SY, Abrazinski TA, Manice LA, Colvin RA, Luster AD. Chemokine receptor CXCR3 and its ligands CXCL9 and CXCL10 are required for the development of murine cerebral malaria. Proc Natl Acad Sci USA. 2008; 105:4814–4819. [PubMed: 18347328]
6. Vandercappellen J, Van Damme J, Struyf S. The role of CXC chemokines and their receptors in cancer. Cancer Lett. 2008; 267:226–244. [PubMed: 18579287]
7. Mohrs M, Shinkai K, Mohrs K, Locksley RM. Analysis of type 2 immunity in vivo with a bicistronic IL-4 reporter. Immunity. 2001; 15:303–311. [PubMed: 11520464]
8. Berg LJ. Signalling through TEC kinases regulates conventional versus innate CD8(+) T-cell development. Nat Rev Immunol. 2007; 7:479–485. [PubMed: 17479128]
9. Dubois S, Waldmann TA, Müller JR. ITK and IL-15 support two distinct subsets of CD8+ T cells. Proc Natl Acad Sci USA. 2006; 103:12075–12080. [PubMed: 16880398]
10. Hu J, Sahu N, Walsh E, August A. Memory phenotype CD8+ T cells with innate function selectively develop in the absence of active Itk. Eur J Immunol. 2007; 37:2892–2899. [PubMed: 17724684]
11. Itsumi M, Yoshikai Y, Yamada H. IL-15 is critical for the maintenance and innate functions of self-specific CD8(+) T cells. Eur J Immunol. 2009; 39:1784–1793. [PubMed: 19544306]
12. Cho H, Choi HJ, Xu H, Felio K, Wang CR. Nonconventional CD8+ T cell responses to *Listeria* infection in mice lacking MHC class Ia and H2-M3. J Immunol. 2011; 186:489–498. [PubMed: 21098224]
13. Xu H, DiIulio NA, Fairchild RL. T cell populations primed by hapten sensitization in contact sensitivity are distinguished by polarized patterns of cytokine production: interferon gamma-producing (Tc1) effector CD8+ T cells and interleukin (Il) 4/Il-10-producing (Th2) negative regulatory CD4+ T cells. J Exp Med. 1996; 183:1001–1012. [PubMed: 8642241]
14. Nakajima C, Mukai T, Yamaguchi N, Morimoto Y, Park WR, Iwasaki M, Gao P, Ono S, Fujiwara H, Hamaoka T. Induction of the chemokine receptor CXCR3 on TCR-stimulated T cells: dependence on the release from persistent TCR-triggering and requirement for IFN-gamma stimulation. Eur J Immunol. 2002; 32:1792–1801. [PubMed: 12115663]
15. Belkaid Y, Von Stebut E, Mendez S, Lira R, Caler E, Bertholet S, Udey MC, Sacks D. CD8+ T cells are required for primary immunity in C57BL/6 mice following low-dose, intradermal challenge with*Leishmania major*. J Immunol. 2002; 168:3992–4000. [PubMed: 11937556]

16. Campanella GS, Medoff BD, Manice LA, Colvin RA, Luster AD. Development of a novel chemokine-mediated in vivo T cell recruitment assay. J Immunol Methods. 2008; 331:127–139. [PubMed: 18206159]

17. Barbi J, Oghumu S, Lezama-Davila CM, Satoskar AR. IFN-gamma and STAT1 are required for efficient induction of CXC chemokine receptor 3 (CXCR3) on CD4+ but not CD8+ T cells. Blood. 2007; 110:2215–2216. [PubMed: 17785588]

18. Uppaluri R, Sheehan KC, Wang L, Bui JD, Brotman JJ, Lu B, Gerard C, Hancock WW, Schreiber RD. Prolongation of cardiac and islet allograft survival by a blocking hamster anti-mouse CXCR3 monoclonal antibody. Transplantation. 2008; 86:137–147. [PubMed: 18622291]

19. Marques CP, Kapil P, Hinton DR, Hindinger C, Nutt SL, Ransohoff RM, Phares TW, Stohlman SA, Bergmann CC. CXCR3-dependent plasma blast migration to the central nervous system during viral encephalomyelitis. J Virol. 2011; 85:6136–6147. [PubMed: 21507985]

20. Lord GM, Rao RM, Choe H, Sullivan BM, Lichtman AH, Luscinskas FW, Glimcher LH. T-bet is required for optimal proinflammatory CD4+ T-cell trafficking. Blood. 2005; 106:3432–3439. [PubMed: 16014561]

21. Dhanji S, Teh HS. IL-2-activated CD8+CD44high cells express both adaptive and innate immune system receptors and demonstrate specificity for syngeneic tumor cells. J Immunol. 2003; 171:3442–3450. [PubMed: 14500639]

22. Dhanji S, Chow MT, Teh HS. Self-antigen maintains the innate antibacterial function of self-specific CD8 T cells in vivo. J Immunol. 2006; 177:138–146. [PubMed: 16785508]

23. Kamanaka M, Kim ST, Wan YY, Sutterwala FS, Lara-Tejero M, Galán JE, Harhaj E, Flavell RA. Expression of interleukin-10 in intestinal lymphocytes detected by an interleukin-10 reporter knockin tiger mouse. Immunity. 2006; 25:941–952. [PubMed: 17137799]

24. Wan YY, Flavell RA. Identifying Foxp3-expressing suppressor T cells with a bicistronic reporter. Proc Natl Acad Sci USA. 2005; 102:5126–5131. [PubMed: 15795373]

25. Meiser A, Mueller A, Wise EL, McDonagh EM, Petit SJ, Saran N, Clark PC, Williams TJ, Pease JE. The chemokine receptor CXCR3 is degraded following internalization and is replenished at the cell surface by de novo synthesis of receptor. J Immunol. 2008; 180:6713–6724. [PubMed: 18453591]

26. Liu N, Phillips T, Zhang M, Wang Y, Opferman JT, Shah R, Ashton-Rickardt PG. Serine protease inhibitor 2A is a protective factor for memory T cell development. Nat Immunol. 2004; 5:919–926. [PubMed: 15311278]

27. Zhang M, Park SM, Wang Y, Shah R, Liu N, Murmann AE, Wang CR, Peter ME, Ashton-Rickardt PG. Serine protease inhibitor 6 protects cytotoxic T cells from self-inflicted injury by ensuring the integrity of cytotoxic granules. Immunity. 2006; 24:451–461. [PubMed: 16618603]

28. Allie SR, Zhang W, Fuse S, Usherwood EJ. Programmed death 1 regulates development of central memory CD8 T cells after acute viral infection. J Immunol. 2011; 186:6280–6286. [PubMed: 21525385]

29. Parish IA, Kaech SM. Diversity in CD8(+) T cell differentiation. Curr Opin Immunol. 2009; 21:291–297. [PubMed: 19497720]

30. Hänninen A, Maksimow M, Alam C, Morgan DJ, Jalkanen S. Ly6C supports preferential homing of central memory CD8+ T cells into lymph nodes. Eur J Immunol. 2011; 41:634–644. [PubMed: 21308682]

31. Carroll HP, Paunovic V, Gadina M. Signalling, inflammation and arthritis: crossed signals: the role of interleukin-15 and -18 in autoimmunity. Rheumatology (Oxford). 2008; 47:1269–1277. [PubMed: 18621751]

32. Miyazaki T, Liu ZJ, Kawahara A, Minami Y, Yamada K, Tsujimoto Y, Barsoumian EL, Permutter RM, Taniguchi T. Three distinct IL-2 signaling pathways mediated by bcl-2, c-myc, and lck cooperate in hematopoietic cell proliferation. Cell. 1995; 81:223–231. [PubMed: 7736574]

33. Waldmann TA. The biology of interleukin-2 and interleukin-15: implications for cancer therapy and vaccine design. Nat Rev Immunol. 2006; 6:595–601. [PubMed: 16868550]

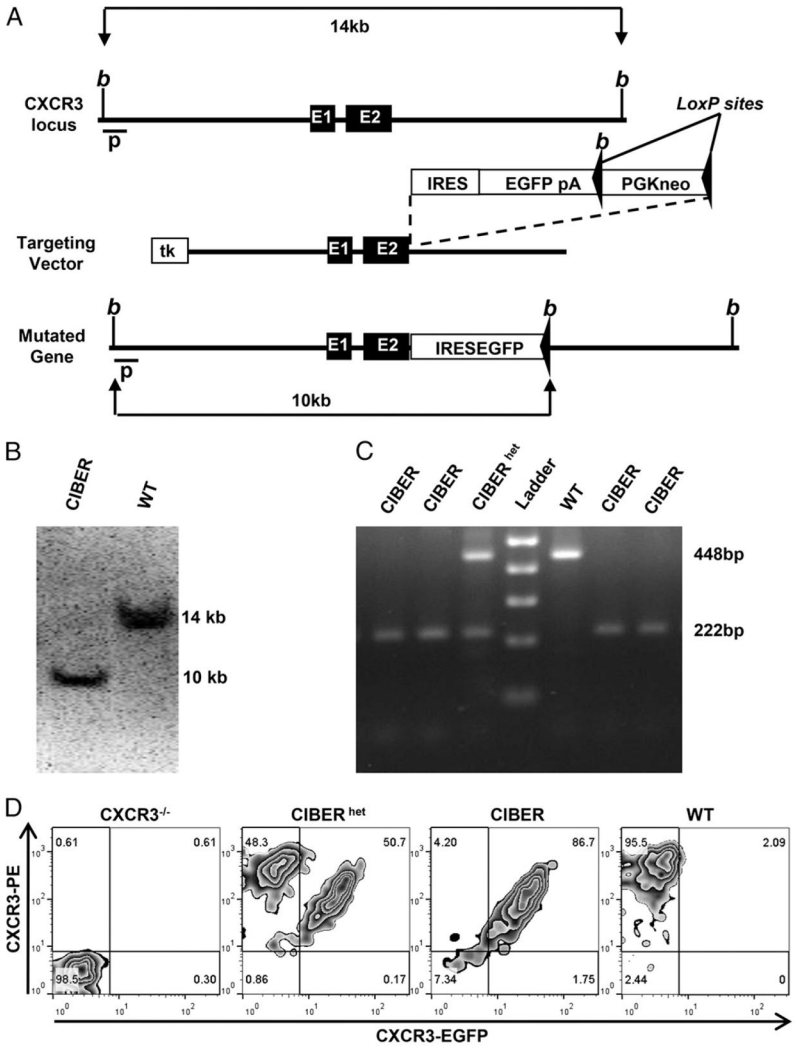

FIGURE 1.

Generation of CIBER mice and validation of GFP production by CXCR3-expressing cells. (**A**) Targeting vector for generation of CIBER mouse and Southern blot strategy for detection of targeted integration into the CXCR3 locus. (**B**) Southern blot screen of genomic DNA from embryonic stem cells electroporated with linearized targeting vector. (**C**) PCR genotyping of genomic DNA from mouse tails of WT, homozygous (CIBER), or heterozygous (CIBER^{het}) mice. (**D**) CXCR3 production by activated splenic T cells of WT, *cxcr3*$^{-/-}$, CIBER, or CIBER^{het} mice. T cells were activated in vitro with plate-bound anti-CD3/CD28 Abs and subsequently recultured in conditioned media. CXCR3 expression is determined by PE-conjugated anti-CXCR3 Ab and fluorescent EGFP production. Experiment was repeated six times. *b*, *BamH1* site; E1, exon 1; E2, exon 2; p, probe; tk, thymidine kinase gene cassette.

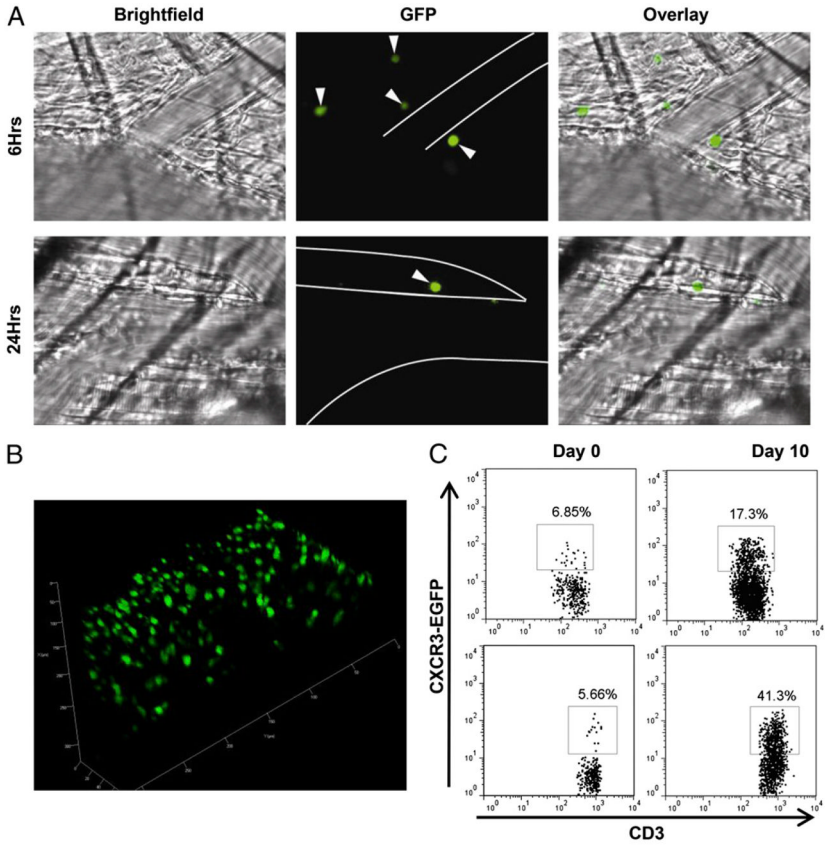

FIGURE 2.

Detection of CXCR3-expressing cells in inflamed tissues in vivo in CIBER mice. (**A**) Representative intravital microscopic images of inflamed cremasteric tissue of male CIBER mice induced by a DNFB-mediated CHS model. Fluorescent images were acquired with an exposure time of 2500 ms. White arrowheads represent GFP cells; white lines outline the vessel wall. Original magnification ×400. (**B**) Representative confocal microscopic image of an inflamed ear of a CIBER mouse induced by DNFB-mediated CHS. Fluorescent images were acquired as Z-stacks using a Zeiss LSM 700 confocal laser-scanning microscope, and three-dimensional images were generated using Zen software (Carl Zeiss MicroImaging GmbH). (**C**) Representative dot plots of CXCR3-expressing T cells in Peyer's patches (*top panels*) and lungs (*bottom panels*) of CIBER mice infected orally with *S. typhimurium* and intranasally with *H. capsulatum*, respectively. T cells are gated on $CD3^+$ lymphocytes. Numbers represent percentages of $EGFP^+$ T cells. Original magnification ×200.

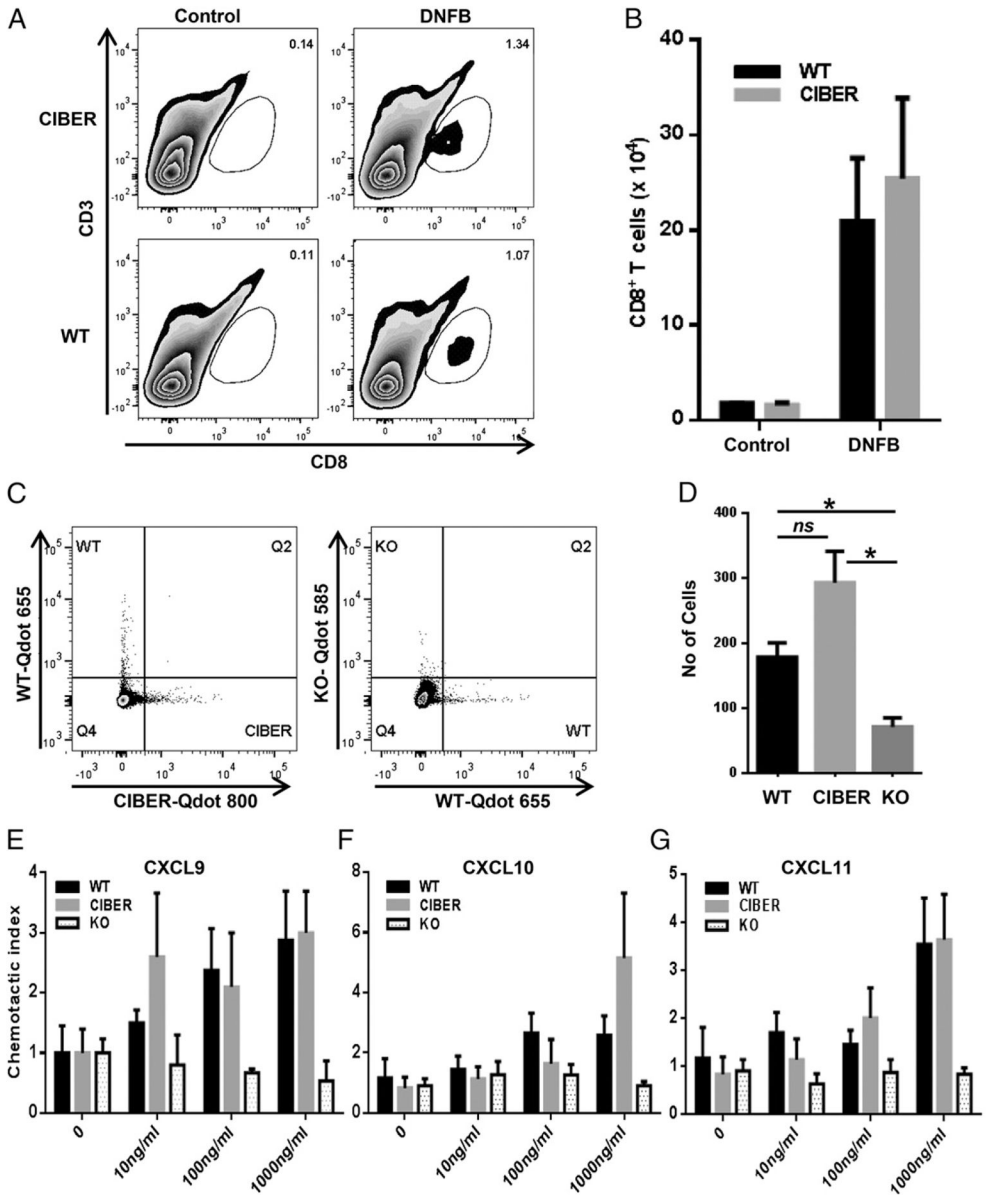

FIGURE 3.

Migration of CXCR3-expressing cells is not compromised in CIBER mice. (**A**) Representative flow cytometric plots of $CD8^+$ T cells migrating to inflamed ear tissue after DNFB-induced CHS in WT and CIBER mice. Numbers represent percentages of $CD8^+$ T cells. (**B**) Graph showing total number of $CD8^+$ T cells migrating to inflamed ear tissue after DNFB-induced CHS in WT and CIBER mice. (**C**) Representative dot plots of labeled and adoptively transferred $CXCR3^+$ T cells from WT and CIBER mice, as well as T cells from *cxcr3*$^{-/-}$ mice recruited to the lungs after administration of chemokine CXCL10. (**D**) Graph showing the average number of labeled and adoptively transferred $CXCR3^+$ T cells from WT and CIBER mice, as well as T cells from *cxcr3*$^{-/-}$ mice recruited to the lungs after administration of the CXCR3 ligand CXCL10. *p <0.05. (**E–G**) In vitro migration of $CXCR3^+$ T cells from WTand CIBER mice, as well as T cells from *cxcr3*$^{-/-}$ mice to the chemokines CXCL9 (E), CXCL10 (F), and CXCL11 (G) using a transwell migration assay.

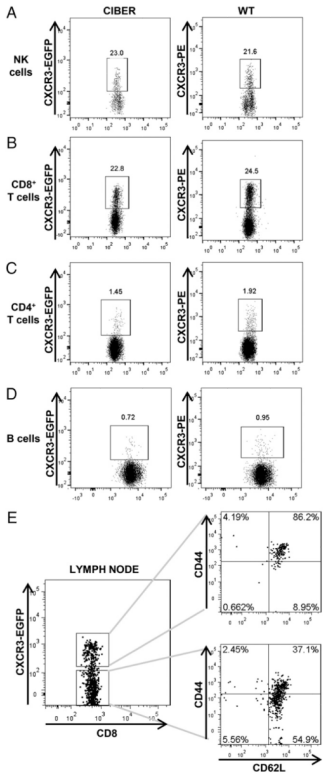

FIGURE 4.

Identification of CXCR3-expressing cells in naive CIBER mice. (**A**–**D**) Representative dot plots showing CXCR3 expression in NK cells (A), $CD8^+$ T cells (B), $CD4^+$ T cells (C), and B cells (D) on lymph nodes of naive CIBER and WT mice. (**E**) Expression of CD44 and CD62L in $CXCR3^+$ and $CXCR3^-$ $CD8^+$ T cells in lymph nodes of naive CIBER mice. All experiments were performed at least three times.

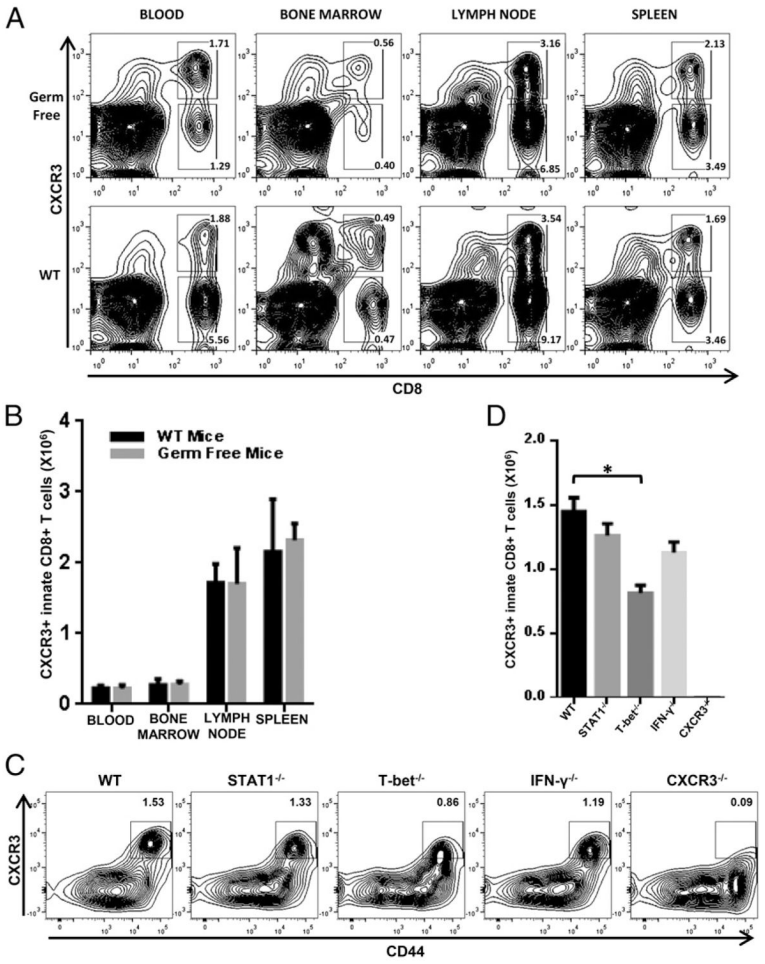

FIGURE 5.

Role of STAT1, IFN-γ, and T-bet in CXCR3 expression by innate CD8$^+$ T cells. (**A**) Identification of CXCR3-expressing and non-expressing innate CD8$^+$ T cells in blood and lymphoid organs of WT and germ-free mice. Numbers correspond to the percentage of CXCR3$^+$ or CXCR3$^-$ in innate CD8$^+$ T cell populations. (**B**) Total numbers of CXCR3$^+$ innate CD8$^+$ T cells in blood and lymphoid organs of WT and germ-free mice. (**C**) Representative flow cytometric plots of CXCR3$^+$ innate CD8$^+$ T cell populations in the spleens of WT, *stat1*$^{-/-}$, T-*bet*$^{-/-}$, *ifn-γ*$^{-/-}$, and *cxcr3*$^{-/-}$ mice. Numbers correspond to the percentage of CXCR3$^+$ innate CD8$^+$ T cell populations. Cells are gated on CD8$^+$, CD3$^+$ lymphocytes. (**D**) Total number of CXCR3$^+$ innate CD8$^+$ T cells in the spleens of WT, *stat1*$^{-/-}$, T-*bet*$^{-/-}$, *ifn-γ*$^{-/-}$, and *cxcr3*$^{-/-}$ mice. *$p < 0.05$.

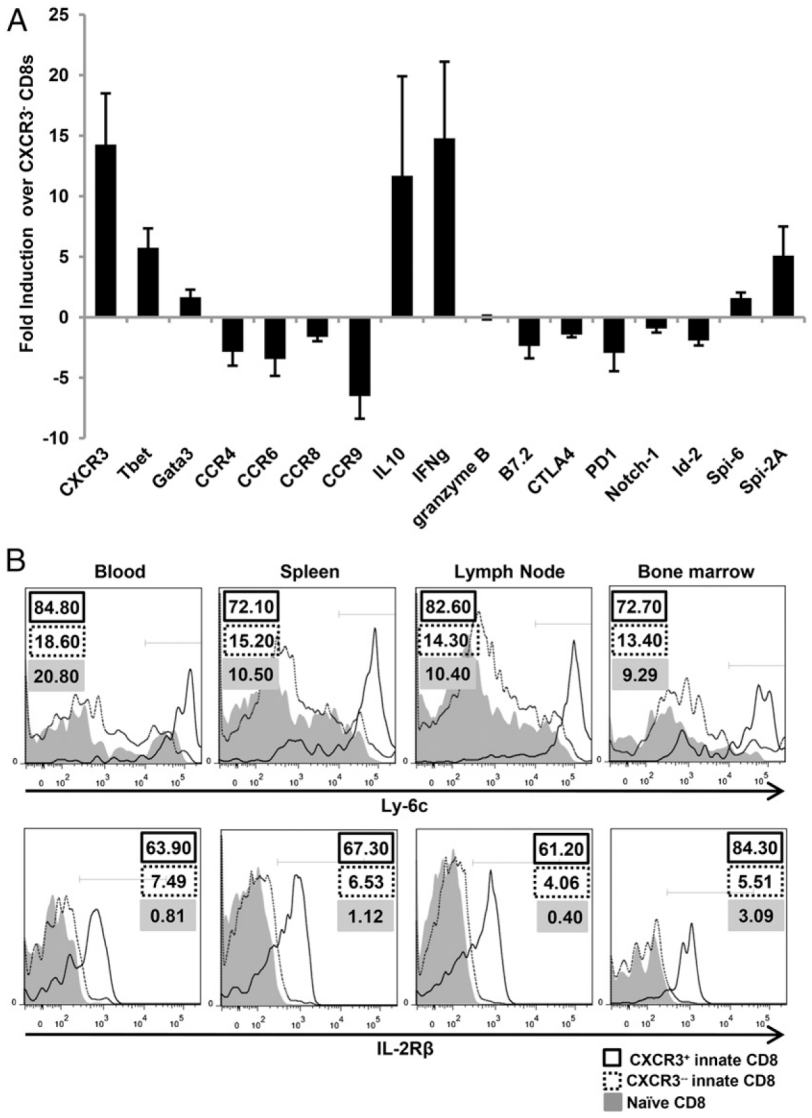

FIGURE 6.

CXCR3$^+$ and CXCR3$^-$ innate CD8$^+$ T populations possess distinct phenotypic characteristics. (**A**) Real-time PCR analysis of sorted innate CD8 T cells from naive CIBER mice. Data are presented as fold induction of CXCR3$^+$ relative to CXCR3$^-$ innate CD8$^+$ T cell populations. Error bars represent SEM from four separate experiments. (**B**) Representative histogram showing surface Ly6C (*top panels*) and IL-2Rβ (*bottom panels*) expression of CXCR3$^+$ and CXCR3$^-$ innate CD8 T cells and naive CD8 T cells. Innate CD8 T cell populations are gated on CD3$^+$ CD8$^+$ CD44$^+$ CD62L$^+$. Naive CD8$^+$ T cells are gated on CD3$^+$ CD8$^+$ CD44$^-$ CD62L$^+$. All experiments were performed at least three times.

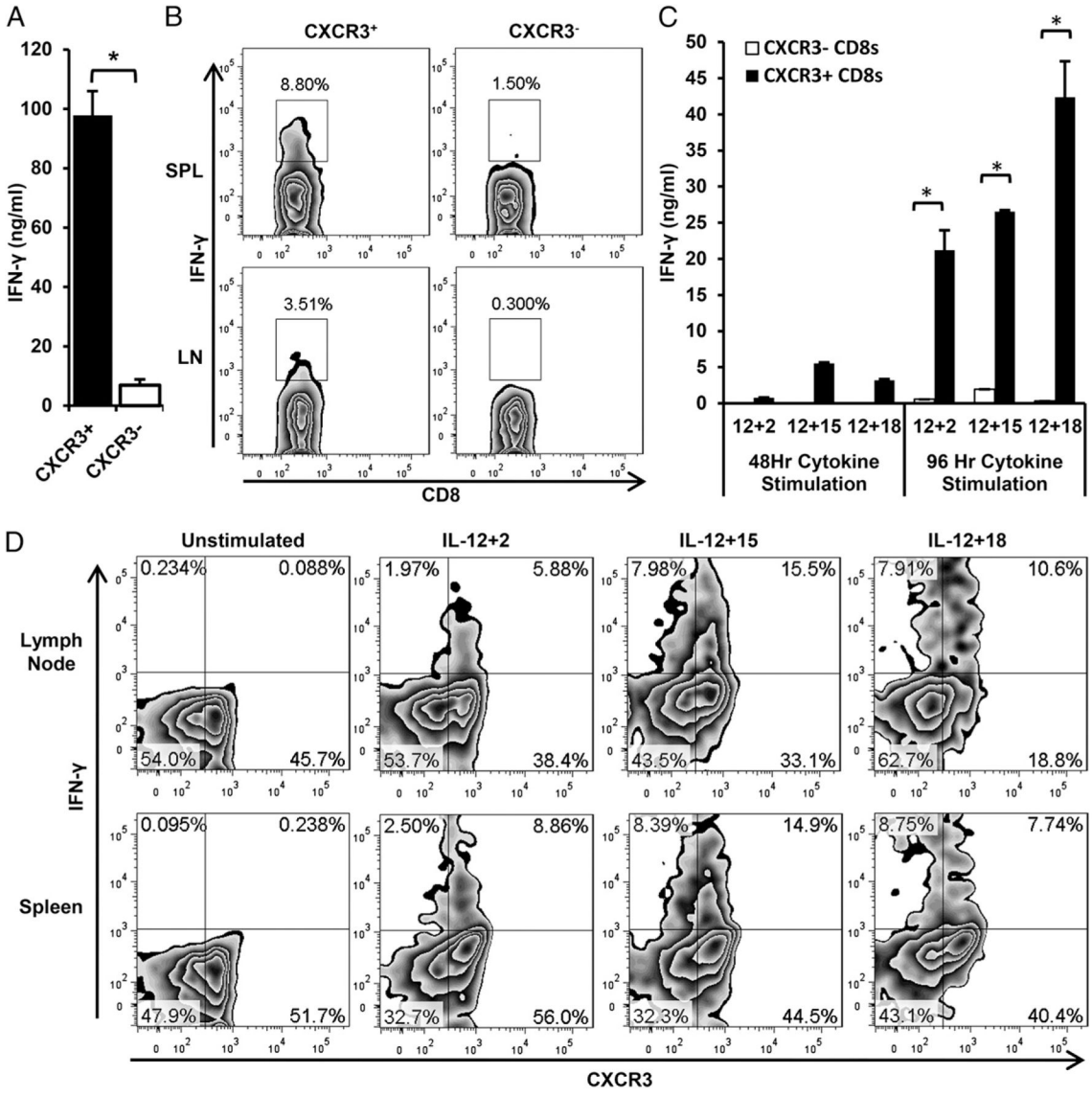

FIGURE 7.

CXCR3$^+$ innate CD8$^+$ T cells produce greater levels of IFN-γ on stimulation. (**A**) IFN-γ levels as determined by cytokine ELISA of sorted CXCR3$^+$ and CXCR3$^-$ innate CD8$^+$ T cells stimulated with anti-CD3/CD28. (**B**) Intracellular IFN-γ production of splenocytes and lymph node cells from CIBER mice stimulated with PMA and ionomycin, as determined by flow cytometry. Cells are gated on innate CD8$^+$ T cells. (**C**) Cytokine ELISA of IFN-γ from FACS-sorted CXCR3$^+$ (filled bars) and CXCR3$^-$ (open bars) innate CD8$^+$ T cells after stimulation with mixed cytokines. (**D**) Flow cytometric density plot showing intracellular IFN-γ production by stimulated CXCR3$^+$ and CXCR3$^-$ innate CD8$^+$ T cells from lymph nodes (*top panels*) and spleens (*bottom panels*) of CIBER mice. Cells were stimulated with IL-12/2, IL-12/15, or IL-12/-18 cytokine combinations. Numbers represent percentage of innate CD8$^+$ T cells in each quadrant. Error bars represent SEM. All experiments were performed at least three times. *$p < 0.01$.

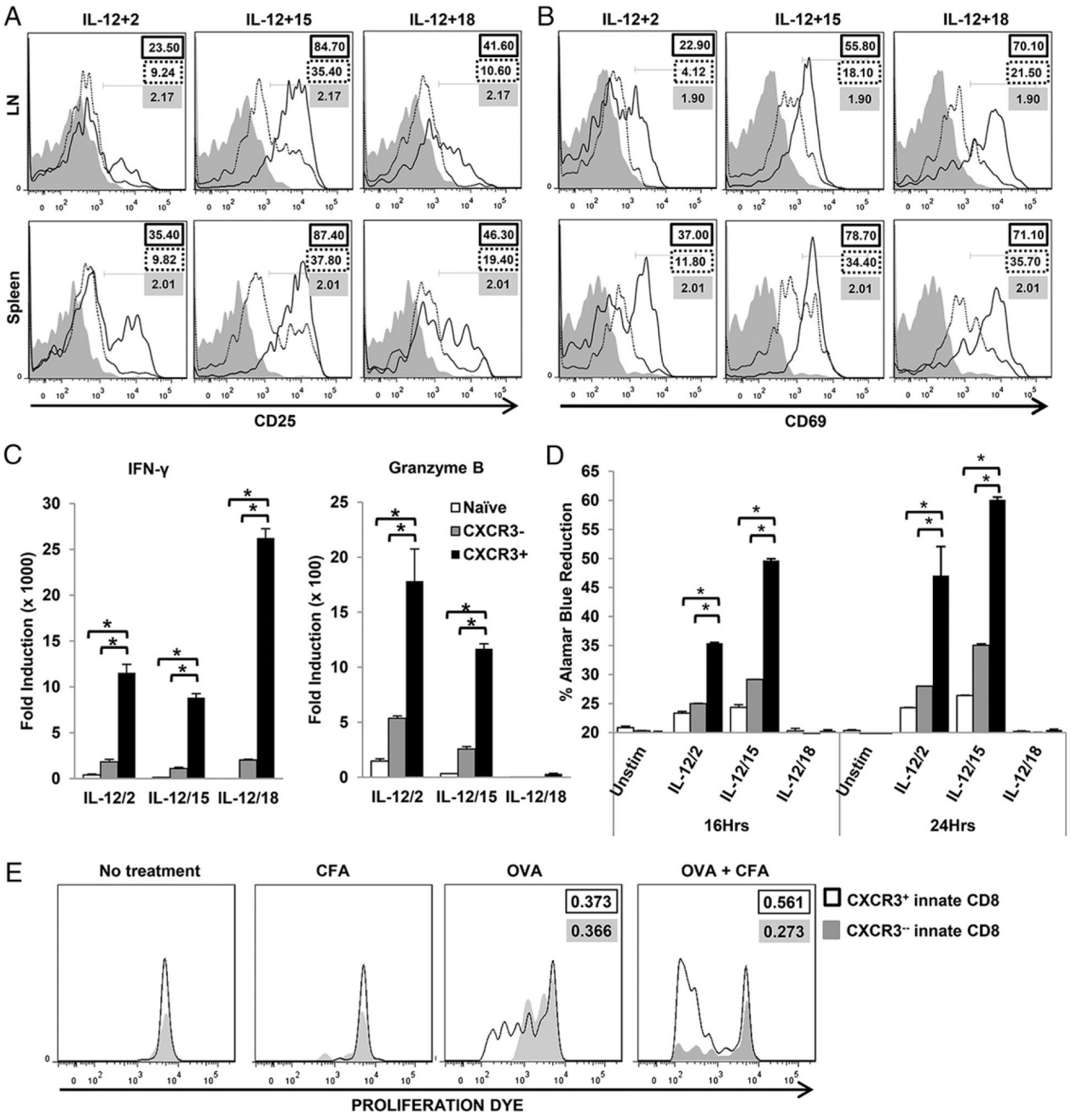

FIGURE 8.

CXCR3$^+$ innate CD8$^+$ T cells proliferate more robustly and produce greater levels of activation markers on stimulation. Expression of (**A**) CD25 and (**B**) CD69 in lymph node cells and splenocytes of naive CIBER mice after stimulation with indicated cytokine combinations. Innate CD8$^+$ T cell populations are gated on CD3$^+$ CD8$^+$ CD44$^+$ CD62L$^+$. Naive CD8$^+$ T cells are gated on CD3$^+$ CD8$^+$ CD44$^-$ CD62L$^+$. (**C**) Real-time PCR analysis of IFN-γ and granzyme B gene expression from sorted CXCR3$^+$ and CXCR3$^-$ innate CD8$^+$ T cells, and naive CD8$^+$ T cells after in vitro cytokine stimulation. Data are presented as fold induction over unstimulated cells. (**D**) Cellular proliferation of sorted CXCR3$^+$ and CXCR3$^-$ innate CD8$^+$ T cells and naive CD8$^+$ T cells stimulated in vitro with mixed

cytokines. Proliferation is determined by reduction of alamarBlue. (**E**) Proliferation of sorted and adoptively transferred $CXCR3^+$ and $CXCR3^-$ innate $CD8^+$ T cells stimulated in vivo with OVA. Proliferation is determined using CellTrace Violet proliferation kit. Numbers represent division index. Error bars represent SEM. All experiments were performed at least three times. $*p < 0.01$.

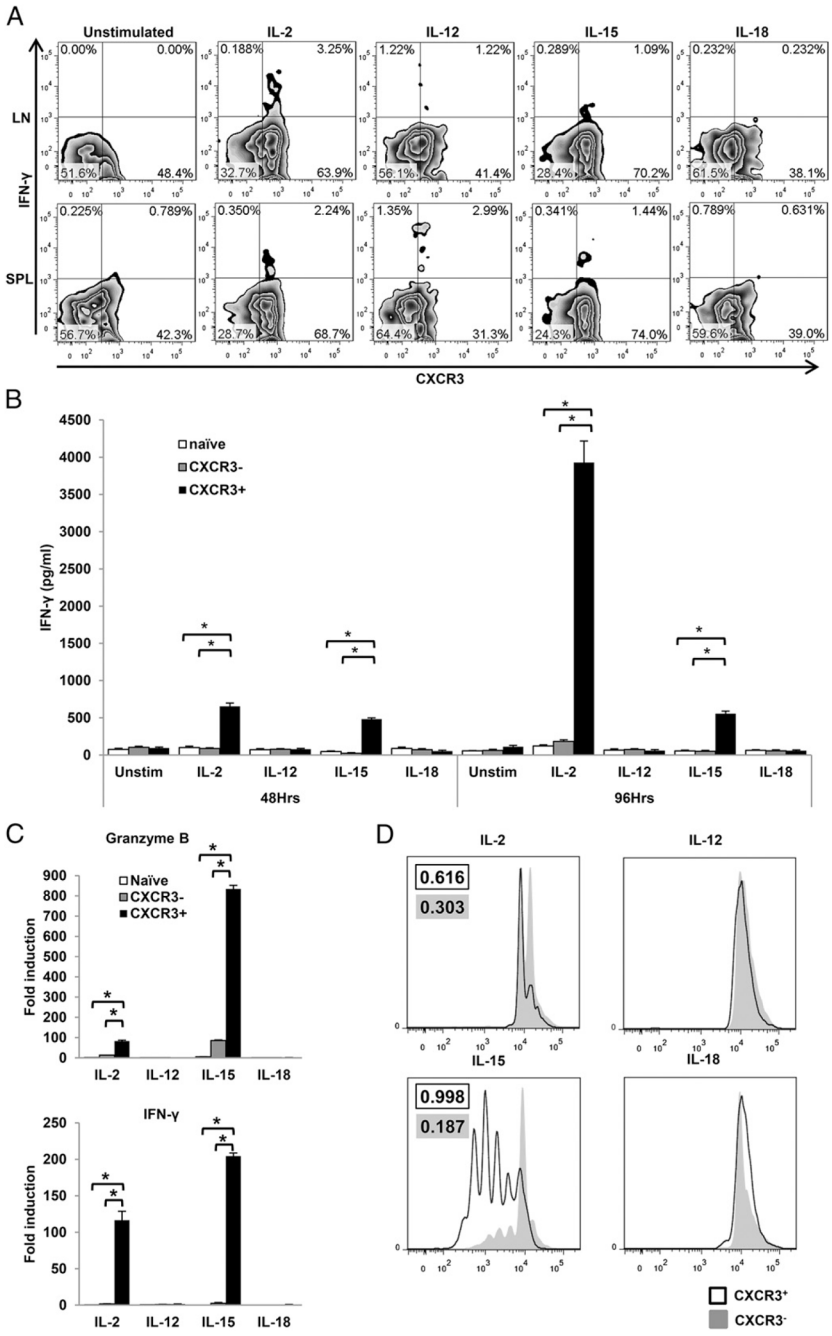

FIGURE 9.

IL-2 and IL-15 enhance the effector functions of CXCR3-expressing innate CD8$^+$ T cells. (**A**) Intracellular IFN-γ produced by lymph node cells and splenocytes obtained from naive CIBER mice and treated with individual cytokines in vitro. Innate CD8 T cell populations are gated on CD3$^+$ CD8$^+$ CD44$^+$ CD62L$^+$. (**B**) IFN-γ levels of sorted CXCR3$^+$ and CXCR3$^-$ innate CD8$^+$ T cells stimulated in vitro with individual cytokines determined by cytokine ELISA. (**C**) Real-time PCR analysis of IFN-γ and granzyme B gene expression from sorted CXCR3$^+$ and CXCR3$^-$ innate CD8$^+$ T cells, and naive CD8$^+$ T cells after individual cytokine stimulation. Data are presented as fold induction over unstimulated cells. (**D**) Cellular proliferation of sorted CXCR3$^+$ and CXCR3$^-$ innate CD8$^+$ T cells and naive

$CD8^+$ T cells stimulated in vitro with individual cytokines. Proliferation is determined using CellTrace Violet proliferation kit. Numbers represent division index. Error bars represent SEM. All experiments were performed at least three times. *$p < 0.01$.